DOI: 10.1002/ejic.201100840

Controllable Synthesis of Single-Crystalline Fe_3O_4 Nanorice by a One-Pot, Surfactant-Assisted Hydrothermal Method and Its Properties

Ramesh Rajendran,*[a] Rajalakshmi Muralidharan,[b] Ramya Santhana Gopalakrishnan,[c] Muthamizhchelvan Chellamuthu,*[a] Suruttaiya U. Ponnusamy,[a] and Elayaperumal Manikandan[d]

Keywords: Hydrothermal synthesis / Nanostructures / Nanoparticles / Magnetic properties / Vibrational properties / Magnetite

Single-crystalline Fe_3O_4 nanorice has been prepared by a simple one-pot, surfactant-assisted hydrothermal method using dodecyltrimethylammonium bromide (DTAB) as a surfactant. X-ray powder diffraction, field emission scanning electron microscopy (FESEM), TEM, high-resolution (HR)-TEM, micro-Raman spectroscopy and magnetic measurements have been employed to study the properties of the product. The importance of NaAc and ethylene glycol in the formation of the pure magnetite phase has been established. The as-synthesized products have a regular rice-like shape with an average diameter of 150 nm and length of 500 nm and are monodisperse. Shape evolution from cauliflower- to rice-like morphology has been achieved by controlling the DTAB concentration. A possible formation mechanism for the Fe_3O_4 nanorice is explored. Furthermore, the product showed ferromagnetic properties at room temperature.

Introduction

In recent years, the size- and shape-dependent properties of nanocrystals (NCs) have been intensively studied due to their varied applications.[1,2] Magnetic nanostructured materials have received intensive attention due to their vital application in numerous areas such as ferrofluids,[3] medical diagnostics,[4] advanced magnetic materials,[5] catalysts,[6] colored pigments,[7] and high-density magnetic recording media.[8] Among magnetic materials, magnetite (Fe_3O_4) is particularly important because of its potential in biomedical applications such as magnetic resonance imaging[9] and targeted drug delivery.[10] To date, differently shaped Fe_3O_4 NCs such as rods,[11] wires,[12] tubes,[13] pyramids,[14] octahedra,[15] rings,[16] triangles,[17] flowers,[18] and spheres[19] have been synthesized. Different synthetic routes, such as reverse micelles, decomposition of organometallics, and solvo- or hydrothermal treatment, have been employed to fabricate Fe_3O_4 NCs with different morphologies. 1D Fe_3O_4 nanostructures such as nanorods and wires have potential applications in biomedicine, such as drug/gene delivery and targeting applications, because of their more efficient interaction with biological entities than spherical nanoparticles.[20] Furthermore, nanocylinders have been used more effectively for drug delivery than their spherical counterparts because they persist in the circulation for longer after intravenous injection. There are only a few reports on the synthesis of rice-like nanostructures. Wang et al. have reported the highly tunable plasmon resonances of α-Fe_2O_3/Au core/shell nanorices (NRs) synthesized through the seed-mediated growth of Au on spindle-type α-Fe_2O_3 nanoparticles.[21] Liang et al. have reported the synthesis of rice-shaped silver nanocrystals with a uniform size distribution by the polyol process.[22] Rebolledo et al. have reported the two-step synthesis of superparamagnetic NRs by thermal reduction of FeOOH obtained by the aerobic oxidation of $FeSO_4$ solutions.[20] Zhang et al. have reported that a spindle-like Fe_3O_4 mesoporous nanostructure was successfully synthesized by reducing the spindle-like α-Fe_2O_3 NPs, which were prepared by forced hydrolysis.[23] No reports are currently available on the one-step synthesis of rice-like Fe_3O_4 NCs with a uniform size distribution. For the first time we report the synthesis of single crystalline Fe_3O_4 NRs with uniform size distribution through a facile surfactant-assisted hydrothermal method. We have explored a simple and efficient method for the synthesis of controlled morphologies with well-defined shape and size for Fe_3O_4 NCs.

[a] Centre for Materials Science and Nano Devices, Department of Physics, SRM University,
Kattankulathur - 203, Chennai, India
Fax: +91-4427452343,
E-mail: rameshphys@gmail.com (for R. R.);
selvancm@gmail.com (for C. M.)
[b] Condensed Matter Physics Division, Indira Gandhi Centre for Atomic Research,
Kalpakkam - 603102, India
[c] Corrosion Science and Technology Division, Indira Gandhi Centre for Atomic Research,
Kalpakkam - 603102, India
[d] National Centre for Nano-Structured Materials, Council for Scientific and Industrial Research,
Pretoria 0001, South Africa
Supporting information for this article is available on the WWW under http://dx.doi.org/10.1002/ejic.201100840.

The surfactant-assisted hydrothermal method is effective for shape- and size-controlled synthesis of single phase Fe_3O_4 NCs without using an inert atmosphere. Li et al. have reported the synthesis of single-crystalline Fe_3O_4 triangular nanoprisms (TNPs) by a surfactant-assisted hydrothermal method using 1,3-propanediamine (PDA) as the surfactant and ethylene glycol (EG) as the reaction medium.[17] It was found that the EG/PDA volume ratio played an important role in the formation of the TNPs and evolution of the morphology of the Fe_3O_4 nanoparticles. In this study, we have used dodecyltrimethylammonium bromide (DTAB) as a surfactant and EG and water as the reaction medium. The concentration of DTAB has been varied and was found to play a crucial role in controlling the evolution of the morphology of the Fe_3O_4 nanoparticles.

Results and Discussion

Structural Study

The phase formation of the product was identified by powder XRD. Figure 1 shows the powder XRD pattern of the Fe_3O_4 NRs. The diffraction peaks are quite similar to those of bulk Fe_3O_4 and can be indexed as the face-centered cubic (FCC) structure of Fe_3O_4 with a lattice constant a = 8.397 Å, which is consistent with the standard data file (JCPDS file no. 82-1533). No diffraction peaks from any impurities were observed, which indicates the high purity of the products. During the hydrothermal synthesis $NaAc{\cdot}3H_2O$ may react with $FeCl_3{\cdot}3H_2O$ to form the intermediate product $Fe(Ac)_3$, which is easily decomposed into Fe_3O_4 in the presence of EG. No resultant product was obtained without addition of $NaAc{\cdot}3H_2O$ in the reaction medium. The α-Fe_2O_3 phase was obtained when water was used as a solvent instead of EG and water under the same reaction conditions. Hence, EG and NaAc were crucial for the synthesis of the Fe_3O_4 phase under hydrothermal conditions.

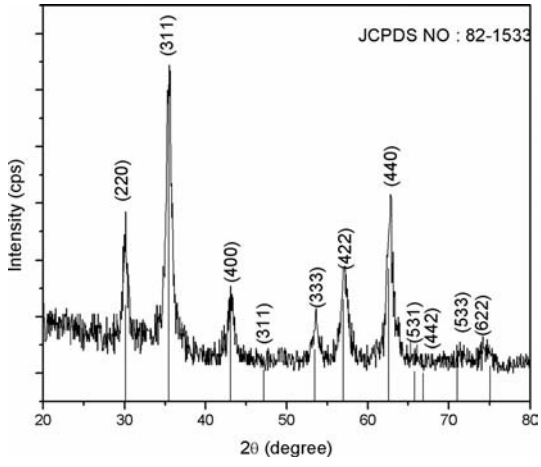

Figure 1. X-ray diffraction pattern of Fe_3O_4 NRs.

Morphology

The morphology of the Fe_3O_4 product was examined by field emission scanning electron microscopy (FESEM) and TEM. Figure 2 (a–c) show high magnification images of the sample obtained at 200 °C for 12 h with DTAB (0.75 g). The surface morphology of the nanorice with an average diameter of about 150 nm and length of about 500 nm was observed. The energy dispersive X-ray spectrum (EDX, Figure 2, d) further confirms the presence of Fe and O in the product (C is from the substrate). The TEM image of the product (Figure 3, a) also shows rice-like morphology, which confirms the observation from the FESEM images. Figure 3 (b) shows a HRTEM image that exhibits a continuous lattice strip, which confirms the single-crystalline nature of the material. From the HRTEM image an interplanar spacing of 0.49 nm was calculated, which corresponds to the (111) plane of Fe_3O_4. From the spot-like selected area electron diffraction (SAED) pattern, it was concluded that the nanoparticles were single crystals and the growth direction was along the [111] direction. Figure 4 (a, b) show the FESEM and TEM images of the product synthesized without DTAB. This product exhibits cauliflower-like architectures, which are composed of 7 nm spherical nanoparticles. An elongated spherical nanostructure was

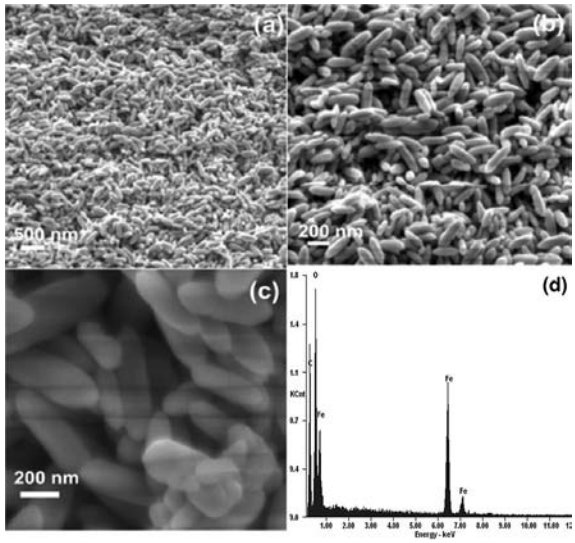

Figure 2. a–c: FESEM images with different magnifications. d: EDX spectrum of Fe_3O_4 NRs.

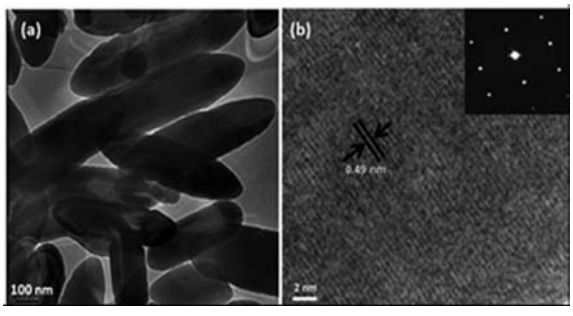

Figure 3. TEM and HRTEM image of Fe_3O_4 NRs.

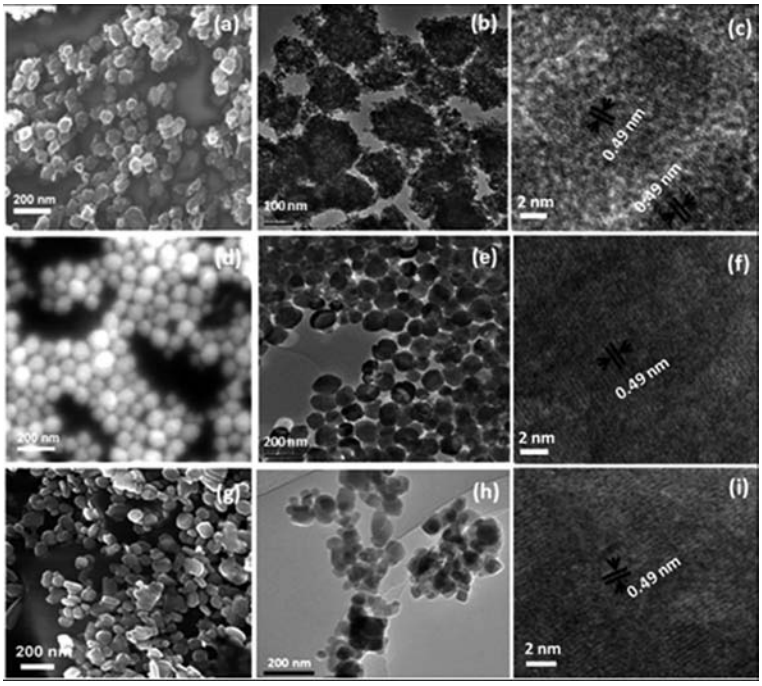

Figure 4. a: FESEM, b: TEM, and c: HRTEM image of cauliflower-like nanoparticles (without DTAB). d: FESEM, e: TEM, and f: HRTEM image of elongated spherical Fe_3O_4 nanoparticles (0.25 g of DTAB). g: FESEM, h: TEM, and i: HRTEM image of polyhedra and rice-like nanoparticles (0.5 g of DTAB).

obtained when the amount of DTAB was 0.25 g (Figure 4, d and f). Increasing the amount of DTAB to 0.5 g led to a product that consisted mostly of polyhedra with a few rice-like nanostructures (Figure 4, g and h). Parts c, f, and i of Figure 4 show HRTEM images of the cauliflower-like, polyhedral, and elongated spherical nanostructures. The lattice plane could be assigned to the (111) plane of Fe_3O_4 with a lattice spacing of 0.49 nm.

Formation Mechanism

The synthesis of rice-like Fe_3O_4 nanoparticles could be useful for biomedical applications. Therefore, we designed a simple, nontoxic, and economically viable route using EG and water as the reaction medium and DTAB as the surfactant. In order to understand the growth mechanism of the Fe_3O_4 NRs, control experiments were performed by varying the concentration of DTAB and keeping the other conditions constant, i.e. the concentration of the Fe^{3+} source, solvent, reaction time, and temperature. The shape transformation in the nanostructures is mainly derived from the capping of DTAB on certain facets. From a crystal growth point of view, the reduction in surface energy is the primary driving force for simple particle growth, and the evolution of morphology is driven by the further reduction of surface energy due to minimization of the area of high surface-energy faces.[24] From a crystallographic point of view, the magnetite is a cubic inverse spinel structure with oxygen anions that form FCC close packing in an ···ABCABC··· sequence along the [111] direction. The Fe ions are located at the tetrahedral sites and octahedral interstitial sites so the activity in the [111] direction is much higher than that in the [100] direction.[25] As has already been reported, the sequence for the variation of surface energies of FCC Fe_3O_4 is $\gamma\{111\} < \gamma\{100\} < \gamma\{110\}$,[26] as {111} facets have the highest atomic density and less open sites for the head group of DTAB to attach to. Whereas, {100} facets have lower atomic density, and the centers of the octahedral interstitial sites of the lattice are located on the plane, which offers more open sites to attract DTAB.[27] The high surfactant coverage on the {100} facets constitutes a barrier to further growth. Figure 5 shows the morphology evolution of Fe_3O_4 NCs with respect to DTAB concentration. In the absence of DTAB, only cauliflower-like products were obtained, which are composed of nanoparticles with a diameter of about 7 nm. The cauliflower-like Fe_3O_4 nanostructure was formed through the oriented attachment of the primary individual particles to minimize their surface energy and magnetic dipole alignment. With the addition of a small amount of DTAB (0.25 g), the product was mainly composed of elongated spheres. The shape transformation from small spherical nanoparticles to elongated spheres is attributed to the effective capping of DTAB on the {100} facets, which caused the growth in the [111] direction to be rapid in comparison to that from the {100} facets. As the amount of DTAB was increased to 0.5 g, the product consisted mostly of polyhedra with a few rice-like Fe_3O_4 nanostructures. This is because the amount of capping agent was increased on the {100} facet, which effectively inhibits growth, so the growth tends to proceed along the [111] direction. The rice-like structures tended to form as single crystals with higher amounts of surfactant (0.75 g) because

of the more effective surfactant barrier on the {100} facets of Fe_3O_4. Furthermore, the influence of reaction time was investigated. When a short reaction time of 3 h was used, an irregular aggregation of nanoparticles was obtained (see Supporting Information, Figure S1a). This is because the time was not sufficient to produce rice-like crystals. By increasing the reaction time to 8 h, aggregated rice-like nanostructures were obtained (Figure S1b). A uniform distribution of Fe_3O_4 nanorice was achieved when the reaction time was 15 h (Figure S1b).

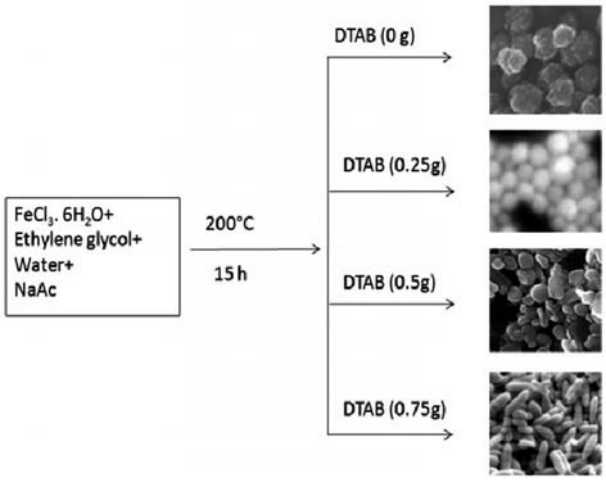

Figure 5. Morphology evolution Fe_3O_4 NCs with respect to DTAB concentration.

Vibratonal Properties

Two reaction media were used to synthesize the Fe_3O_4 nanostructures: (i) a mixture of water and EG and (ii) water alone. In the first case, a Fe_3O_4 phase was obtained, whereas in water alone an α-Fe_2O_3 phase was obtained. To identify the phase of the nanostructures, micro-Raman spectra of the products were recorded. Raman spectroscopy is a powerful tool to distinguish between Fe_3O_4 and α-Fe_2O_3 phases. Fe_3O_4 has a *Fd3m* space group, in which half of the Fe^{3+} cations are located on tetrahedral (A) sites, and the other Fe^{3+} and all of the Fe^{2+} cations are randomly distributed on the octahedral (B) sites. According to space group symmetry and factor group analysis, the optical phonon modes are distributed over the symmetry species of the *Fd3m* group as $C = 5T_{1u} + A_{1g} + E_g + 3T_{2g}$.[28] Of these, five are IR-active vibrations ($5T_{1u}$) and five are Raman-active vibrations (A_{1g}, E_g and $3T_{2g}$). Figure 6 (a–d) shows micro-Raman spectra of the Fe_3O_4 samples synthesized with various amounts of DTAB. The predominant peak seen at 670 cm^{-1} in all the spectra represents the A_{1g} vibration mode of Fe_3O_4, which is consistent with the reported value for single-crystalline and nanophase Fe_3O_4.[29,30] Figure 6 (d) corresponds to the spectrum of the Fe_3O_4 nanorice and shows the predominant peak at 670 cm^{-1} in addition to peaks at 474 and 538 cm^{-1}, which are assigned to the T_{2g} (2) and T_{2g} (3) modes of Fe_3O_4, respectively.[31] The peaks at 832 cm^{-1} and in the range 1115–1130 cm^{-1} are not related to iron oxide and represent DTAB bound to the surface. The intensity of these bands increased with the increasing amount of DTAB. Figure S2 shows the micro-Raman spectrum of the nanostructures produced in water alone, which shows the predicted Raman modes of α-Fe_2O_3 nanoparticles. The formation of Fe_3O_4 from reactions with EG and water and α-Fe_2O_3 from those with water alone was confirmed by Raman measurements. It was concluded that EG is crucial for the formation of a single phase of Fe_3O_4.

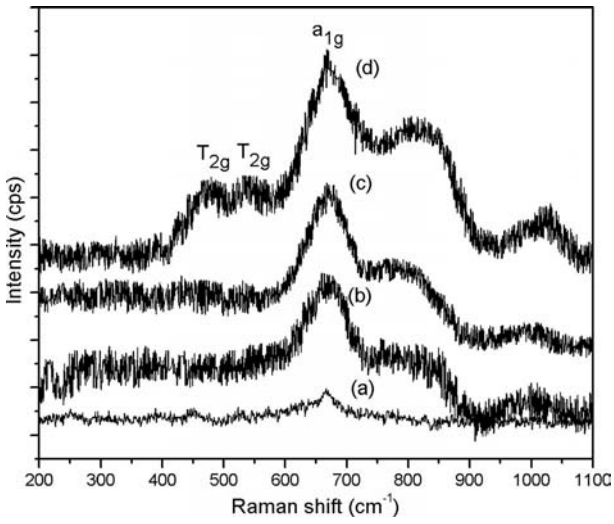

Figure 6. Micro-Raman spectra of a: cauliflower-like, b: elongated spherical, c: polyhedra and rice-like, and d: rice-like Fe_3O_4 nanostructures.

Magnetic Properties

Figure 7 shows the magnetization curve of the Fe_3O_4 nanomaterials at room temperature. All the synthesized products show a hysteresis loop, which implies their ferromagnetic nature. The magnetic properties of the synthesized products with respect to their different morphologies are listed in Table S1 and show that the magnetic properties are sensitive to the crystal size and morphology of the sample. The saturation magnetization (M_s) values of the samples are smaller than those of the bulk materials (92 emu g^{-1}). It is well known that the magnetic properties of materials are greatly influenced by many factors, such as size, structure, morphology, crystallinity, and crystal defects.[32–34] The M_s value of the cauliflower-like nanostructures is lower than that of the spherical, polyhedral, and rice-like nanoparticles, which may be attributed to the smaller crystal size (7 nm) of the nanoparticles. As shown in Table S1, the H_c and M_r values of Fe_3O_4 nanorice were higher than those of the cauliflower-like, spherical, and polyhedral nanoparticles. The increased H_c value is attributed to the shape and magnetocrystalline anisotropy of the 1D nanostructures. It has been reported that an increase in the H_c and M_r values of a 1D nanostructure are due to an increase in both mag-

netocrystalline and shape anisotropy, which exert an influence on the magnetic properties. Shape anisotropy can increase the coercivity, which arises from the alignment of the magnetic spins along the long axis and to reverse the direction requires more energy for long particles than for other shapes.[35]

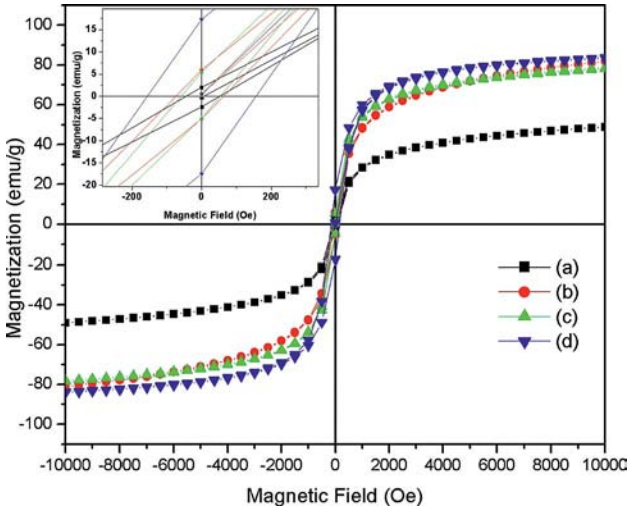

Figure 7. Magnetization curves of a: cauliflower-like, b: elongated spherical, c: polyhedran and rice-like, and d: rice-like Fe_3O_4 nanostructures.

Conclusions

We have synthesized Fe_3O_4 NRs by a facile one-pot, surfactant-assisted hydrothermal method by variation of the concentration of DTAB. The morphology evolution of the NCs was investigated by varying the DTAB concentration and reaction time. The proposed formation mechanism for the NRs was that capping DTAB molecules on the {100} facets of the FCC structure resulted in the inhibition of growth along a particular crystallographic direction and increased the tendency for growth along the [111] direction. The room temperature magnetization measurements show that the NCs have ferromagnetic properties. Such Fe_3O_4 NRs could be of interest for applications in biomedicine.

Experimental Section

Materials and Method: All reagents were of analytical grade and used without further purification. In a typical procedure, $FeCl_3 \cdot 6H_2O$ (0.9 g) was dissolved in EG (20 mL) and distilled water (20 mL) to form a clear solution. CH_3COONa (1.9 g) and DTAB (0.75 g) were added with stirring. The mixture was stirred for one hour and transferred to a 50 mL Teflon®-lined autoclave. The autoclave was sealed and maintained at 200 °C for 15 h before being allowed to reach room temperature. The black precipitate was collected by centrifugation, washed several times with distilled water and absolute ethanol, and dried in vacuo at 60 °C overnight. Cauliflower-like, elongated spherical, and polyhedral Fe_3O_4 nanoparticles were synthesized by using 0 g, 0.25 g, and 0.5 g of DTAB, respectively, keeping all other conditions constant.

Characterization: XRD patterns were recorded with a powder X-ray diffractometer (X′Pert PRO MPD, Panalytical, Cu-K_α radiation, λ = 0.154178 nm). The morphology of the samples was inspected using a Quanta 200 FEG scanning electron microscope (FESEM). TEM and HRTEM images and SAED patterns were measured by TEM. One drop of the magnetic fluid was placed on a carbon coated copper grid, dried in vacuo and the TEM image was taken with a JEM 2100 (JEOL) transmission electron microscope with an accelerating voltage of 200 kV. Size analysis from the TEM images was performed using image processing software ImageJ. Micro-Raman measurements were carried out with an HR 800 (Jobin–Yvon) Raman microscope equipped with a 1,800 grooves/mm holographic grating. A He–Ne laser of 633 nm was used as an excitation source. The laser spot size focused on the surface was approximately 3 μm, and the depth resolution was 0.5 μm. The output of the filtered He–Ne laser was 5 mW. The magnetization measurements were performed with a VSM JDM-13 vibrating sample magnetometer. All the measurements were performed at room temperature.

Supporting Information (see footnote on the first page of this article): The aggregation of nanoparticles obtained from different reaction times, the micro-Raman spectrum of the nanostructures produced in water alone, the magnetic properties of the synthesized products with respect to their different morphologies.

Acknowledgments

R. R. would like to thank SRM University for financial support and the Nanotechnology Research Center for FESEM characterization. The authors also thank Dr. A. K. Arora, Dr. B. V. R. Tata, and Dr. C. S. Sundar (IGCAR) for support and encouragement.

[1] N. Tian, Z. Y. Zhou, S.-G. Sun, Y. Ding, Z. L. Wang, *Science* **2007**, *316*, 732–735.
[2] D. J. Hornbaker, S. J. Kahng, S. Misra, B. W. Smith, A. T. Johnson, E. J. Mele, D. E. Luzzi, A. Yazdani, *Science* **2002**, *295*, 828–831.
[3] M. T. Lopez-Lopez, J. D. Duran, A. Delgado, F. Gonzalez-Caballero, *J. Colloid Interface Sci.* **2005**, *291*, 144–151.
[4] J. W. M. Bulte, D. L. Kraitchman, *NMR Biomed.* **2004**, *17*, 484–499.
[5] Z. M. Liao, Y. D. Li, J. Xu, J. M. Zhang, K. Xia, D. P. Yu, *Nano Lett.* **2006**, *6*, 1087–1091.
[6] W. Werner, R. Wolfgang, *Prog. Surf. Sci.* **2002**, *70*, 4741–4747.
[7] J. H. Meng, G. Q. Yang, L. M. Yan, X. Y. Wang, *Dyes Pigm.* **2005**, *66*, 109–113.
[8] C. T. Black, C. B. Murray, R. L. Sandstrom, S. Sun, *Science* **2000**, *290*, 1131–1134.
[9] Y. Tian, B. Yu, X. Li, K. Li, *J. Mater. Chem.* **2011**, *21*, 2476–2481.
[10] F. H. Chen, L. M. Zhang, Q. T. Chen, Y. Zhang, Z. J. Zhang, *Chem. Commun.* **2010**, *46*, 8633–8635.
[11] S. Xuan, F. Wang, Y.-X. J. Wang, J. C. Yu, K. C.-F. Leung, *J. Mater. Chem.* **2010**, *20*, 5086–5094.
[12] H. Singh, S. Bhagwat, S. Jouen, B. Lefez, A. A. Athawale, B. Hannoyer, S. Ogale, *Phys. Chem. Chem. Phys.* **2010**, *12*, 33246–3253.
[13] C. Terrier, M. Abid, C. Arm, S. Serrano-Guisan, L. Gravier, J.-Ph. Ansermet, *J. Appl. Phys.* **2005**, *98*, 086102–086102–3.
[14] B. Geng, F. Zhan, H. Jiang, Y. Guo, Z. Xing, *Chem. Commun.* **2008**, *44*, 5773–5775.
[15] S. V. Pol, V. G. Pol, A. Gedanken, I. Felner, M. G. Sung, S. Asai, *Inorg. Chem.* **2007**, *46*, 4951–4959.
[16] X. F. Qu, G. T. Zhou, Q. Z. Yao, S. Q. Fu, *J. Phys. Chem. C* **2010**, *114*, 284–289.

[17] X. Li, Z. Si, Y. Lei, J. Tang, S. Wang, S. Su, S. Song, L. Zhao, H. Zhang, *CrystEngComm* **2010**, *12*, 2060–2063.
[18] B. Lv, Y. Xu, Q. Gao, D. Wu, Y. Sun, *J. Nanosci. Nanotechnol.* **2010**, *10*, 2348–59.
[19] J. Xie, F. Zhang, M. Aronova, L. Zhu, X. Lin, Q. Quan, G. Liu, G. Zhang, K. Choi, K. Kim, X. Sun, S. Lee, S. Sun, R. Leapman, X. Chen, *ACS Nano* **2011**, *5*, 3043–3051.
[20] A. F. Rebolledo, O. B. Miguel, J. F. Marco, P. Tartaj, *Adv. Mater.* **2008**, *20*, 1760–1765.
[21] H. Wang, D. W. Brandl, F. Le, P. Nordlander, N. J. Halas, *Nano Lett.* **2006**, *6*, 827–832.
[22] H. Liang, H. Yang, W. Wang, J. Li, H. Xu, *J. Am. Chem. Soc.* **2009**, *131*, 6068–6069.
[23] S. Zhang, W. Wu, X. Xiao, J. Zhou, F. Ren, C. Jiang, *Nanoscale Res. Lett.* **2011**, *6*, 89.
[24] R. L. Penn, J. F. Banfield, *Geochim. Cosmochim. Acta* **1999**, *63*, 1549–1557.
[25] M. E. Fleet, *Acta Crystallogr., Sect. B: Struct. Crystallogr. Cryst. Chem.* **1981**, *37*, 917.
[26] L. Zhang, R. He, H. C. Gu, *Mater. Res. Bull.* **2006**, *41*, 260–267.
[27] C. Ni, P. A. Hassan, E. W. Kaler, *Langmuir* **2005**, *21*, 3334–3337.
[28] L. V. Gasparov, D. B. Tanner, D. B. Romero, H. Berger, G. Margaritondo, L. Forro, *Phys. Rev. B* **2000**, *62*, 7939–7944.
[29] O. N. Shebanova, P. Lazor, *J. Solid State Chem.* **2003**, *174*, 424–430.
[30] G. V. M. Jacintho, A. G. Brolo, P. Corio, P. A. Z. Suarez, J. C. Rubim, *J. Phys. Chem. C* **2009**, *113*, 7684–7691.
[31] G. V. M. Jacintho, A. G. Brolo, P. Corio, P. A. Z. Suarez, J. C. Rubim, *J. Phys. Chem. C* **2009**, *113*, 7684–7691.
[32] E. P. Valstyn, J. P. Hanton, A. H. Morrish, *Phys. Rev.* **1962**, *128*, 2078.
[33] L. P. Zhu, H. M. Xiao, W. D. Zhang, G. Yang, S. Y. Fu, *Cryst. Growth Des.* **2008**, *8*, 957–963.
[34] J. Lu, X. L. Jiao, D. R. Chen, W. Li, *J. Phys. Chem. C* **2009**, *113*, 4012–4017.
[35] R. Ramesh, A. Ashok, G. M. Bhalero, S. Ponnusamy, C. Muthamizhchelvan, *Cryst. Res. Technol.* **2010**, *45*, 965–968.

Received: August 10, 2011
Published Online: November 4, 2011

